

Thermal conductivity of multi-walled carbon nanotubes: Molecular dynamics simulations*

Hu Guo-Jie(胡帼杰) and Cao Bing-Yang(曹炳阳)[†]

Key Laboratory for Thermal Science and Power Engineering of Ministry of Education, Department of Engineering Mechanics, Tsinghua University, Beijing 100084, China

(Received 17 January 2014; revised manuscript received 21 February 2014; published online 24 July 2014)

Heat conduction in single-walled carbon nanotubes (SWCNTs) has been investigated by using various methods, while less work has been focused on multi-walled carbon nanotubes (MWCNTs). The thermal conductivities of the double-walled carbon nanotubes (DWCNTs) with two different temperature control methods are studied by using molecular dynamics (MD) simulations. One case is that the heat baths (HBs) are imposed only on the outer wall, while the other is that the HBs are imposed on both the two walls. The results show that the ratio of the thermal conductivity of DWCNTs in the first case to that in the second case is inversely proportional to the ratio of the cross-sectional area of the DWCNT to that of its outer wall. In order to interpret the results and explore the heat conduction mechanisms, the inter-wall thermal transport of DWCNTs is simulated. Analyses of the temperature profiles of a DWCNT and its two walls in the two cases and the inter-wall thermal resistance show that in the first case heat is almost transported only along the outer wall, while in the second case a DWCNT behaves like parallel heat transport channels in which heat is transported along each wall independently. This gives a good explanation of our results and presents the heat conduction mechanisms of MWCNTs.

Keywords: multi-walled carbon nanotubes, thermal conductivity, temperature control method, molecular dynamics simulation

PACS: 65.80.-g, 65.80.Ck, 68.90.+g

DOI: 10.1088/1674-1056/23/9/096501

1. Introduction

As a typical kind of low-dimensional materials, carbon nanotubes (CNTs) have many unique mechanical, electrical, optical, and thermal properties, and have attracted much attention due to their promising applications in engineering.^[1] The CNTs are of great interest in related energy applications because of their high thermal conductivity. They have been embedded into polymers or other media to improve the thermal properties of composites,^[2,3] dispersed in fluids to improve their heat transfer properties,^[4,5] and used to coat substrates to enhance the phase transition heat transfer.^[6] Therefore, the thermal properties and heat conduction mechanism of CNTs need to be fully studied.

In recent years, many researchers have obtained the thermal properties of CNTs including single tubes and bulk CNT samples using various methods, such as lattice dynamics analyses,^[7,8] experimental measurements,^[9–17] and MD simulations.^[18–24] Mingo *et al.*^[7] and Wang *et al.*^[8] calculated the thermal conductivity of an SWCNT based on the Boltzmann equations and the Landauer quantum transport formula. Their theoretical studies focused on the physical mechanism gave qualitative conclusions. Mingo *et al.*^[7] showed that the thermal conductivity of a carbon nanotube increases and even diverges as the nanotube length increases. Wang *et al.*^[8] found the thermal conductance is proportional to the di-

ameter for SWCNTs and to the square of diameter for MWCNTs. Fujii *et al.*^[9] and Kim *et al.*^[10] measured the thermal conductivity of single MWCNTs, while Pop *et al.*^[11] and Yu *et al.*^[12] experimentally obtained the thermal conductivity of single SWCNTs. They found that at room temperature the thermal conductivity of a single CNT, SWCNT, or MWCNT, reached $\sim 10^3 \text{ W}\cdot\text{m}^{-1}\cdot\text{K}^{-1}$. Experimental results for bulk CNT samples,^[14–17] including CNT films, CNT ropes, and aligned CNT arrays, have also been reported, but their thermal conductivities were only $15\text{--}500 \text{ W}\cdot\text{m}^{-1}\cdot\text{K}^{-1}$, much lower than the value for a single tube. These experimental measurements gave quantitative conclusions, but the results were not consistent with each other because of the limitations of the experimental techniques and unavoidable errors at nanoscale. The MD simulations^[18–24] have been used to study the effects of various factors on the thermal conductivity of CNTs to offer a better knowledge of their thermal properties. Maruyama^[19] investigated the length dependence of the thermal conductivity of the (5, 5) and (10, 10) SWCNTs, and found that the thermal conductivity of (5, 5) SWCNTs does not converge to a finite value with the increase in tube length, but obeys a striking power law relation. Alaghamandi *et al.*^[20] calculated the thermal conductivity of SWCNTs and MWTNs as a function of the length, temperature, and chiral index, and argued that the thermal conductivity increases with the length, while de-

*Project supported by the National Natural Science Foundation of China (Grant Nos. 51322603, 51136001, and 51356001), the Program for New Century Excellent Talents in University, Science Fund for Creative Research Groups of China (Grant No. 51321002), and the Initiative Scientific Research Program of Tsinghua University, China.

[†]Corresponding author. E-mail: caoby@tsinghua.edu.cn

creases with the temperature at low temperature and then increases as the temperature increases. Moreover, the chiral index was found to be only a weak influence parameter.

However, the results obtained by various methods do not agree well, especially for single MWCNTs. Fujii *et al.*^[9] measured the thermal conductivity of MWCNTs to be about $2800 \text{ W}\cdot\text{m}^{-1}\cdot\text{K}^{-1}$ using a suspended sample-attached T -type nanosensor. Kim *et al.*^[10] reported a measured value of $3000 \text{ W}\cdot\text{m}^{-1}\cdot\text{K}^{-1}$ using the self-heating method. In addition, Alaghamandi *et al.*^[20] predicted the thermal conductivity of an armchair triple-walled carbon nanotube in the range of $26\text{--}134 \text{ W}\cdot\text{m}^{-1}\cdot\text{K}^{-1}$ using MD simulations. Since the definition of the cross-sectional area affects the value of thermal conductivity, all the values mentioned above have been converted to a cross-sectional area of an SWCNT, and each wall of an MWCNT is equal to an annular ring of thickness 0.34 nm . Meanwhile, the existing studies of the influence factors for the thermal conductivity mainly focused on the structure parameters of CNTs but paid little attention on the experimental or simulation conditions except for the temperature, which is believed to influence the thermal conductivity greatly.

In this paper, the influence of the temperature control method on the thermal conductivity of MWCNTs is studied by using MD simulations. Two different temperature control methods are applied. One is that the HBs are imposed only on the outer wall, and the other is that the HBs are imposed on both the two walls. Furthermore, the inter-wall thermal transport of MWCNTs is investigated. Finally, the heat conduction mechanisms of MWCNTs are revealed.

2. Molecular dynamics simulation

Molecular dynamics simulations have been widely used to investigate the thermal conductivity and the heat conduction mechanisms of CNTs^[18–24] because they can not only determine the macroscopic thermal properties but also yield useful atomistic information for analyzing the thermal energy transport in CNTs. The MD methods used to calculate the thermal conductivity are an equilibrium molecular dynamics (EMD) method based on the Green–Kubo formula derived from linear response theory and a nonequilibrium molecular dynamics (NEMD) method based on Fourier’s law of heat conduction, which imposes an external perturbation field,^[25] a temperature difference,^[26] a heat current,^[27] a transient heat impulsion,^[28] internal thermal noise,^[29] or a uniform heat sources and sinks.^[30,31] The EMD method has a higher computational demand than the NEMD scheme, due to the slow convergence of the autocorrelation function and the need of a large ensemble of simulations. Thus, the present work uses the NEMD method to predict the thermal conductivities of the DWCNTs.

As mentioned above, two different temperature control methods (i.e. imposing the HBs only on the outer wall and on both the two walls) are applied. The simulation models with the HBs imposed only on the outer wall and on both the two walls are illustrated in Figs. 1(a) and 1(b), respectively. In both the two cases, each wall of a DWCNT is divided into N slabs along the axial direction. The temperatures of the first and $(1 + N/2)$ th slabs of the outer wall of the DWCNT are kept at $T_L = T_0 - \delta T$ and $T_H = T_0 + \delta T$ in the first case, while those of both the two walls of the DWCNT are kept at T_L and T_H in the second case. Here T_0 is the mean system temperature and δT is the difference between the heat bath temperature and T_0 . The temperatures are kept by the Nose–Hoover thermostat method.^[32,33] In our simulation, T_0 is set to be 300 K and δT equals 30 K . Moreover, periodic boundary conditions are used along the axial direction in both the two cases.

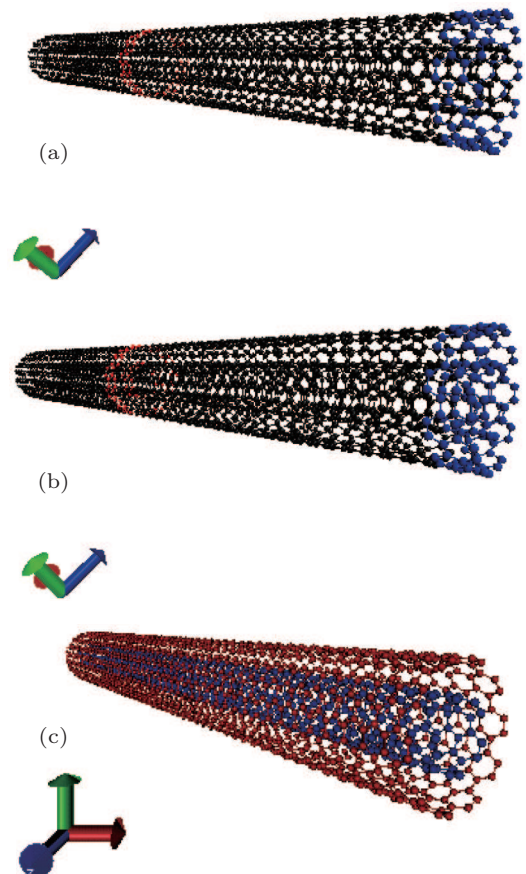


Fig. 1. (color online) Schematics of the simulation models with the HBs imposed (a) only on the outer wall, (b) on both the two walls, and (c) the simulation system modeling the inter-wall heat conduction.

The interactions between the carbon atoms include the intra-wall C–C bond potentials and the inter-wall interactions. The intra-wall C–C bond potentials are modeled by the Brenner potential^[34]

$$E_b = \sum_i \sum_{j(>i)} [V_R(r_{ij}) - B_{ij}V_A(r_{ij})], \quad (1)$$

where E_b is the total C–C bond potential of the system, B_{ij} is the many-body interaction parameter which represents the many-body coupling between the bond from atom i to atom j and the local environment of atom i , V_R and V_A are the repulsive and attractive pair terms, and r_{ij} is the intermolecular distance between atom i and atom j . The inter-wall interactions are based on the Lennard–Jones potential

$$V(r) = 4\epsilon \left[\left(\frac{\sigma}{r} \right)^{12} - \left(\frac{\sigma}{r} \right)^6 \right], \quad (2)$$

where r is the intermolecular distance, $\epsilon = 2.968$ meV is the energy parameter, and $\sigma = 0.3407$ nm is the molecular diameter.^[35] The motion equations for the molecules are integrated using the Leap–Frog algorithm with a time step of $dt = 0.5$ fs. Each case is run for 50000 time steps for the system to reach an equilibrium at the mean temperature, and then for 450000 steps to impose the heat baths on the corresponding positions of the system and to stabilize the heat conduction. After that, the local slab temperatures and heat flux are averaged over 3500000 steps. This time length is sufficient to obtain converged results, as shown below. Based on Fourier’s law of heat conduction, the thermal conductivity is calculated as

$$\lambda = -\frac{q}{\nabla T}, \quad (3)$$

where λ is the thermal conductivity, q is the heat flux, and ∇T is the temperature gradient.

In this paper, three DWCNTs with different chirality pairs are simulated (see Table 1). In order to discuss the results of the DWCNTs, the thermal conductivities of the corresponding SWCNTs are also simulated. The simulation method and the parameters of the HBs are the same as those for the DWCNT. Since the cross-section of an SWCNT or each wall of an MWCNT is an annular ring with a wall thickness of 0.34 nm, its area can be calculated by $S = 2\pi R\delta$, where R is the radius of each wall and δ is the wall thickness. The MWCNT have a cross-sectional area of $S = 2\pi\delta \sum_{i=1}^{n_w} R_i$, where R_i is the radius of the i th wall of the MWCNT, and n_w is the number of walls in the MWCNT.

Table 1. Structure parameters of three DWCNTs.

Chirality pair	Radius/nm	Interwall distance/nm
(5, 5)@(10, 10)	0.344/0.688	0.344
(8, 2)@(17, 2)	0.364/0.718	0.354
(13, 0)@(22, 0)	0.516/0.873	0.357

3. Results and discussion

The temperature profiles of the 6.24-nm (5, 5)@(10, 10) DWCNT and its inner and outer walls with the HBs imposed only on the outer wall and on both the two walls are shown in

Fig. 2. In both the two cases, the temperature jumps near the temperature-controlled sections, i.e., the corresponding slabs of the outer wall in the first case and those of the whole DWCNT in the second case. The jumps can be explained by the existence of localized edge modes (LEMs) and the accumulation of LEM because of the deterministic characteristic of the Nose–Hoover heat bath.

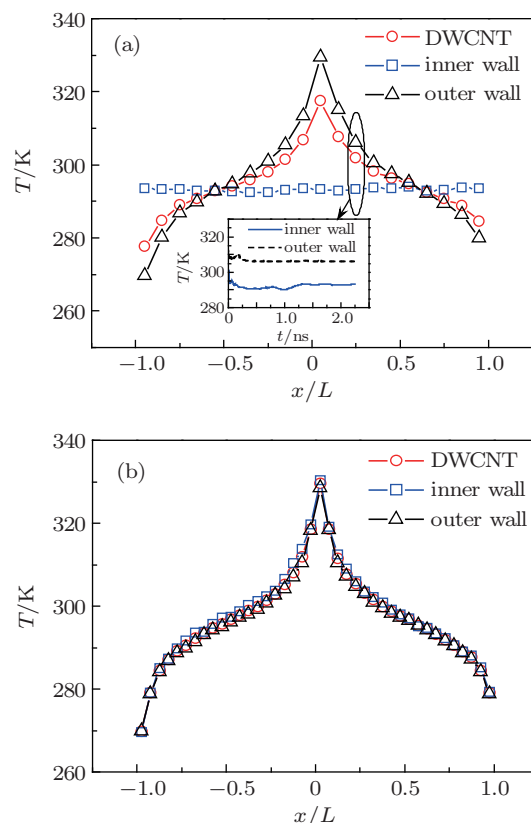


Fig. 2. (color online) Temperature profiles of the 6.24-nm (5, 5)@(10, 10) DWCNT and its inner and outer walls with the HBs imposed only on the outer wall (a) and on both the two walls (b). Insert in panel (a): temperature evolution over time for the inner and outer walls of the DWCNT at the position of $x/L = 0.25$ in the first case.

Figure 2(a) shows the temperature profiles of the DWCNT and its inner and outer walls and temperature evolution over time for the two walls at a certain position in the first case where the HBs are imposed only on the outer wall. It can be seen that the temperatures of the two walls have been stabilized and temperature difference exists between the two walls. Furthermore, there is no temperature gradient in the inner wall of the DWCNT and its temperature is close to the mean system temperature. In the outer wall of the DWCNT, the temperature is approximately linear in the middle sections and the temperature gradient is obtained by a linear fitting of the temperature distribution in the section. The temperature profiles of the DWCNT and its inner and outer walls in the second case with the HBs imposed on both the two walls are presented in Fig. 2(b). As shown in the figure, there are linear temperature distributions in the middle sections for all three profiles and the temperature gradients are obtained by linearly fitting the

temperature distributions. In addition, the three profiles are very similar to each other, especially in the middle linear sections, so the temperature gradients are almost the same. For the other two DWCNTs, i.e., (8, 2)@(17, 2) and (13, 0)@(22, 0) DWCNTs, the temperature profiles exhibit similar characteristics.

Both the great deviation of the profiles of the inner and outer walls of the DWCNT in the first case and the good coincidence of these profiles in the second case interpret that the inter-wall interactions in the DWCNT do not affect the temperature distributions in either wall significantly. In the first case, the outer wall reaches its thermal equilibrium without disturbing the inner wall. In the second case, the two walls reach their own thermal equilibrium. These phenomena are physically reasonable because the inter-wall interactions in DWCNTs are much weaker than the intra-wall interactions. In our calculations, the inter-wall Lennard–Jones potential is at least two orders of magnitude smaller than the intra-wall Brenner potential. The inter-wall thermal resistance will then be relatively large and heat transfer will be mostly along the intra-wall channels. Therefore, heat is conducted only through the outer wall when the HBs are imposed only on the outer wall, while the DWCNT behaves like a parallel heat transport network in which heat is transported along each wall when the HBs are imposed on both the two walls.

In order to verify the analysis of the heat transport behaviors, the heat flows and fluxes of the (5, 5)@(10, 10) DWCNTs

with the HBs imposed only on the outer wall and on both the two walls are obtained, as shown in Fig. 3. Furthermore, the heat flows and fluxes of the (5, 5) and (10, 10) SWCNTs are also presented. In the figures, the zero point of the time axis is set to be the start point of the statistical average process. Initially, when the statistical average process just starts, the curves are wavy since the results of the heat flows and fluxes are basically fluctuating transient values. With the increase in the statistical time, the results are stabilized as shown in the figures, and the values of the heat flows and fluxes used to obtain the thermal conductivity are the stabilized results. It can be seen that the heat flow of the (5, 5)@(10, 10) DWCNT with the HBs imposed only on the outer wall is similar to that of the (10, 10) SWCNT, while the heat flow of the (5, 5)@(10, 10) DWCNT is about the sum of those of the (5, 5) and (10, 10) SWCNTs when the HBs are imposed on both the two walls of the DWCNT. Considering the influence of the cross-sectional area, the heat flux of the (5, 5)@(10, 10) DWCNT with the HBs imposed only on the outer wall is approximate one third smaller than that of the DWCNTs with the HBs on both the two walls, which is almost the same as those of the (5, 5) and (10, 10) SWCNTs. The heat flows and fluxes of the other two DWCNTs, i.e., (8, 2)@(17, 2) and (13, 0)@(22, 0) DWCNTs, and their corresponding SWCNTs have a similar relation. These findings verify the discussion above. When the HBs are imposed only on the outer wall of the DWCNT, heat transports only through the outer wall. When the HBs are imposed on both the two walls, heat is transported along each wall like a parallel heat transport network.

The thermal conductivities of the three DWCNTs, i.e., (5, 5)@(10, 10), (8, 2)@(17, 2), and (13, 0)@(22, 0) DWCNTs, with the HBs imposed only on the outer wall and on both the two walls and their corresponding SWCNTs for different lengths are shown in Fig. 4. Figure 4(a) also shows the MD results for (5, 5) SWCNTs at 300 K by Maruyama^[19] and the theoretical predictions for an (10, 0) SWCNT whose radius is almost equal to (5, 5) at 316 K by Mingo and Broido.^[7] For comparison, all the values in the references are converted to a cross-sectional area of an annular ring of thickness 0.34 nm.

As shown in Fig. 4(a), our present simulation results for the (5, 5) SWCNTs agree well with the previous values,^[7,19] which demonstrates that this analysis can accurately predict the thermal conductivities of CNTs. The thermal conductivities for the (5, 5) and (10, 10) SWCNTs with the same length are almost the same with relative errors mostly less than 15%. Furthermore, comparison of the results for the (5, 5), (10, 10) SWCNTs and (5, 5)@(10, 10) DWCNTs with the HBs imposed on both the two walls with the same length suggests that they have similar thermal conductivities with differences between those for the DWCNTs and the (5, 5), (10, 10) SWCNTs within 10%. Besides, the thermal conductivities of the

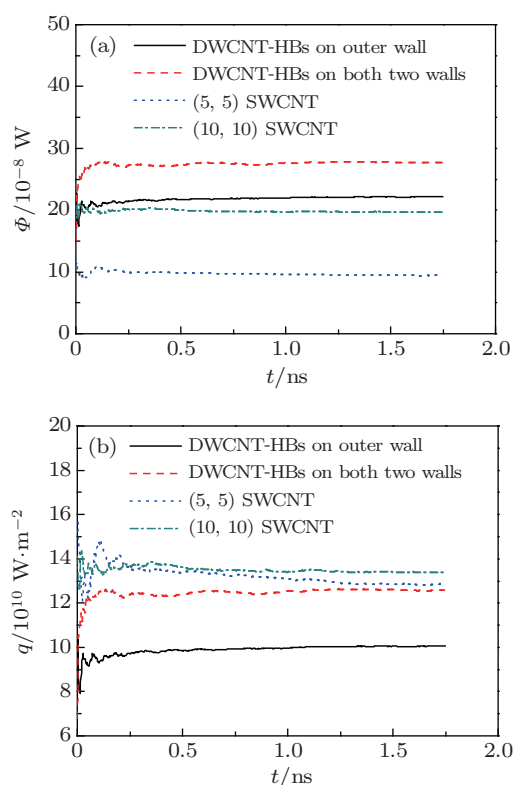


Fig. 3. (color online) Heat flow (a) and flux (b) evolution over time for the 6.24-nm (5, 5)@(10, 10) DWCNTs with the HBs imposed only on the outer wall and on both the two walls and the (5, 5) and (10, 10) SWCNTs.

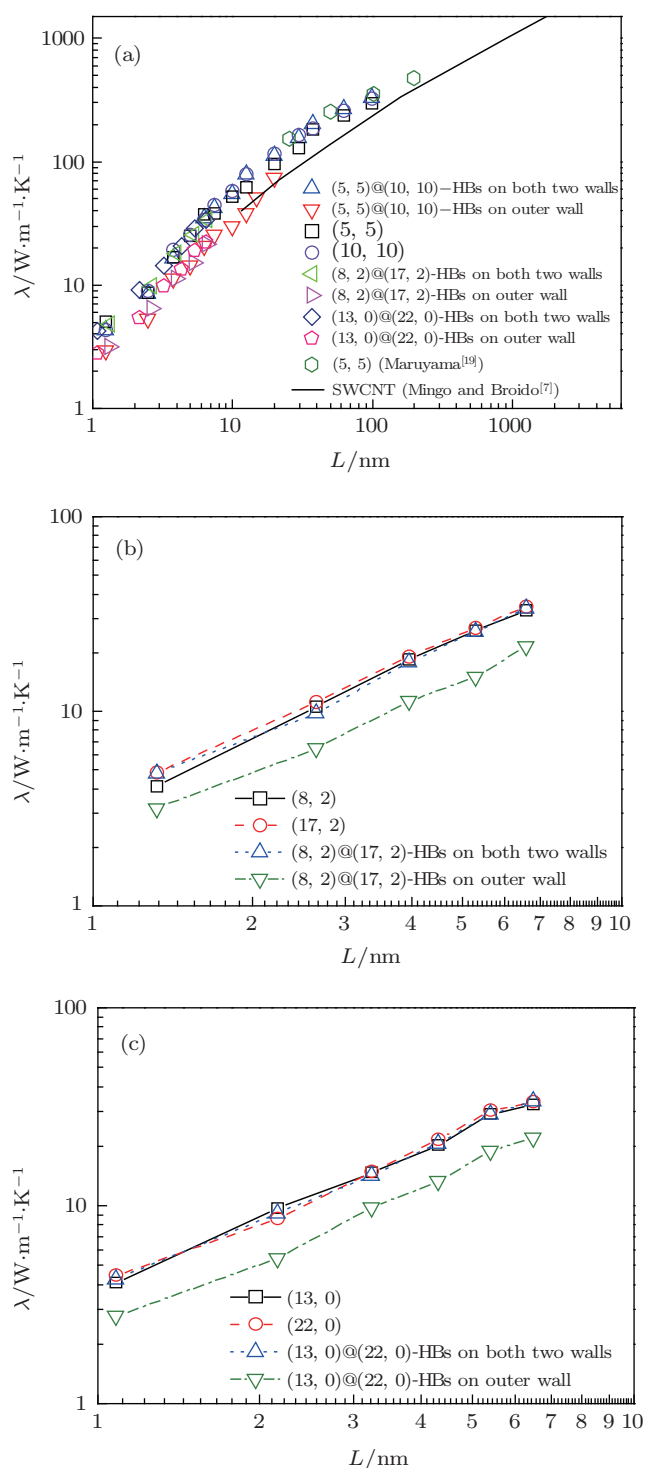


Fig. 4. (color online) Length dependence of the thermal conductivities of the (5, 5)@(10, 10), (8, 2)@(17, 2), and (13, 0)@(22, 0) DWCNTs with the HBs imposed only on the outer wall and on both the two walls and the (5, 5) and (10, 10) SWCNTs (a), (8, 2) and (17, 2) SWCNTs (b), and (13, 0) and (22, 0) SWCNTs at 300 K (c).

(8, 2)@(17, 2) and (13, 0)@(22, 0) DWCNTs are similar to that of the (5, 5)@(10, 10) DWCNTs with the same length, which indicates that the chirality does not influence the thermal conductivity obviously. The conclusion is consistent with the report for SWCNTs.^[20] In Fig. 4(b), it can be seen that the (8, 2), (17, 2) SWCNTs and (8, 2)@(17, 2) DWCNTs with the HBs imposed on both the two walls with the same length

have similar thermal conductivities. In addition, as shown in Fig. 4(c), the (13, 0), (22, 0) SWCNTs and (13, 0)@(22, 0) DWCNTs with the HBs imposed on both the two walls with the same length also have similar thermal conductivities. As discussed before, the temperature profiles shown in Fig. 2(b) which indicates that each DWCNT wall reaches its own thermal equilibrium and heat flow profiles presented in Fig. 3(b) interpreting heat is conducted through both the two walls help explain the results. In the case where the HBs are imposed on both the two walls, the DWCNT is like a set of parallel heat transport channels which conduct heat almost independent of each other, so they independently reach the thermal equilibrium. In addition, the thermal conductivities of the single channels are almost the same, so the thermal conductivity of the DWCNT with its parallel thermal circuits is also the same. Thus, these temperature and heat flow profiles and thermal conductivities are reasonable.

By comparing the thermal conductivities of the (5, 5)@(10, 10) DWCNTs with the HBs imposed only on the outer wall and on both the two walls, as well as the two cases for the (8, 2)@(17, 2) and (13, 0)@(22, 0) DWCNTs, we find that the ratio of the thermal conductivity of the DWCNT in the first case to that in the second case is inversely proportional to the ratio of the cross-sectional area of the DWCNT to that of its outer wall. The temperature profiles shown in Fig. 2(a) and the heat flow profiles presented in Fig. 3(a) give a good explanation. In the case where the HBs are imposed only on the outer wall, the temperature gradient only exists in the outer wall and heat is only transported along the outer wall, which is just like the heat transfer process in the SWCNT corresponding to the outer wall. Since the cross-sectional area of the DWCNT is not equal to that of its outer wall, the ratio of the thermal conductivity of the DWCNT to that of the corresponding SWCNT will be inversely proportional to the ratio of the cross-sectional area of the DWCNT to that of its outer wall. Considering the previous conclusion that the SWCNT corresponding to the outer wall and the DWCNT with the HBs imposed on both the two walls have similar thermal conductivities, we can well interpret the finding that the ratio of the thermal conductivity of the DWCNT with the HBs imposed only on the outer wall to that with the HBs imposed on both the two walls is inversely proportional to the ratio of the cross-sectional area of the DWCNT to that of its outer wall. Besides, the experimental data of an MWCNT by Kim *et al.*^[10] also provide an evidence. Since in the measurement method of self-heating, only the outer wall of the MWCNT is heated, the outer walls made a more significant contribution in thermal transport than the inner walls and the thermal conductivity of the MWCNT that is similar to that of an SWCNT by Pop *et al.*^[11] is inversely proportional to the diameter of the outer walls.

In order to explore the heat conduction mechanisms of DWCNTs more clearly, the inter-wall thermal resistance of the (5, 5)@(10, 10) DWCNTs is investigated by using NEMD simulations. The simulation system is illustrated in Fig. 1(c). The temperatures of the inner and outer walls are maintained at $T_L = T_0 - \delta T$ and $T_H = T_0 + \delta T$, respectively. Here the values of T_0 and δT are also set to be 300 K and 30 K, respectively, and the temperatures are also maintained by the Nose–Hoover thermostat method.^[32,33]

Based on the definition of the thermal resistance at an interface, also known as Kapitza resistance,^[36] the inter-wall thermal resistance of the (5, 5)@(10, 10) DWCNTs is equal to the temperature jump between the two walls divided by the heat flux across the interface. For comparison, the intra-wall axial thermal resistance of each wall is also obtained based on the formula of $R = L/(\lambda \cdot S)$, where S is the cross-sectional area of each wall, and L is the tube length. The inter-wall thermal resistances of the (5, 5)@(10, 10) DWCNTs and intra-wall axial resistances of the two walls for different lengths at 300 K are shown in Fig. 5. It can be seen that the inter-wall resistance decreases with the increasing length, and the values of the resistance are of the order of 10^{10} – 10^{12} K/W, which are of the same order of magnitude as those obtained in the previous MD studies^[37–39] of the thermal resistance between CNTs. Comparison of the three resistances indicates that the inter-wall thermal resistance is at least two orders of magnitude larger than the intra-wall axial resistances. The great values of the inter-wall thermal resistances are physically reasonable as the inter-wall interactions in DWCNTs are much weaker than the intra-wall interactions. The simulation results of the inter-wall thermal resistances confirm our analysis of the heat conduction mechanisms of DWCNTs. Since the inter-wall thermal resistance is very large, almost no heat is transferred in the inter-wall direction. Therefore, heat is transported only along the outer wall when the HBs are imposed only on the outer wall, while the two walls of DWCNTs conduct heat almost independently when the HBs are imposed on both the two walls.

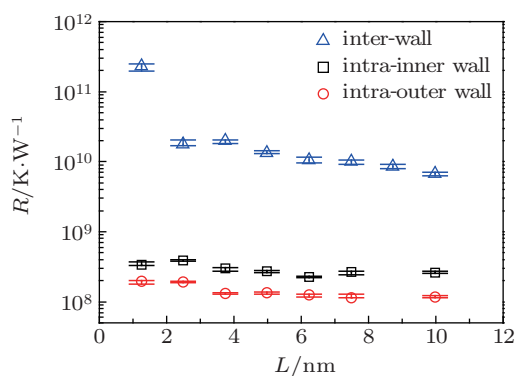


Fig. 5. (color online) Length dependence of the inter-wall thermal resistances of the (5, 5)@(10, 10) DWCNTs and intra-wall axial resistances of the two walls at 300 K.

4. Conclusion

The thermal conductivities of the DWCNTs with two different temperature control methods that impose the HBs only on the outer wall and on both the two walls are investigated by using NEMD simulations. The results show that the ratio of the thermal conductivity of a DWCNT with the HBs imposed only on the outer wall to that with the HBs imposed on both the two walls is inversely proportional to the ratio of the cross-sectional area of the DWCNT to that of its outer wall, and the value for the DWCNT with the HBs imposed on both the two walls is almost the same as those of the corresponding SWCNTs. In order to interpret our results and explore the heat conduction mechanism of MWCNTs, the temperature and heat flow profiles of a DWCNT and its two walls in the two cases are obtained and the inter-wall thermal transport of DWCNTs is simulated. Based on the analyses of the temperature and heat flow profiles and the predicted values of the inter-wall thermal resistances that are of the order of 10^{10} – 10^{12} K/W and at least two orders of magnitude larger than the intra-wall axial resistances, it is explored that heat is almost transported only along the outer wall in the case where the HBs are imposed only on the outer wall, while a DWCNT behaves like parallel heat transport channels in which heat is transported along each wall independently in the case where the HBs are imposed on both the two walls. The present study helps to reveal the heat conduction mechanisms of MWCNTs and provides some better comparable conclusions with the experimental measurement where only the outer walls of the MWCNT make good thermal contacts to a thermal bath.

References

- [1] Baughman R H, Zakhidov A A and de Heer W A 2002 *Science* **297** 787
- [2] Biercuk M J, Llaguno M C, Radosavljevic M, Hyun J K, Johnson A T and Fischer J E 2002 *Appl. Phys. Lett.* **80** 2767
- [3] Alexandrou I, Kymakis E and Amaratunga G A J 2002 *Appl. Phys. Lett.* **80** 1435
- [4] Choi S U S, Zhang Z G, Yu W, Lockwood F E and Grulke E A 2001 *Appl. Phys. Lett.* **79** 2252
- [5] Eastman J A, Phillpot S R, Choi S U S and Keblinski P 2004 *Annu. Rev. Mater. Rev.* **34** 219
- [6] Ujereh S, Fisher T and Mudawar I 2007 *Int. J. Heat Mass Transfer* **50** 4023
- [7] Mingo N and Broido D A 2005 *Nano Lett.* **5** 1221
- [8] Wang J and Wang J S 2006 *Appl. Phys. Lett.* **88** 111909
- [9] Fujii M, Zhang X, Xie H, Ago H, Takahashi K, Ikuta T, Abe H and Shimizu T 2005 *Phys. Rev. Lett.* **95** 065502
- [10] Kim P, Shi L, Majumdar A and McEuen P L 2001 *Phys. Rev. Lett.* **87** 215502
- [11] Pop E, Mann D, Wang Q, Goodson K and Dai H 2006 *Nano Lett.* **6** 96
- [12] Yu C, Shi L, Yao Z, Li D and Majumdar A 2005 *Nano Lett.* **5** 1842
- [13] Chiu H Y, Deshpande V V, Postma H W C, Lau C N, Miko C, Forro L and Bockrath M 2005 *Phys. Rev. Lett.* **95** 226101
- [14] Yi W, Lu L, Zhang D L, Pan Z W and Xie S S 1999 *Phys. Rev. B* **59** 9015
- [15] Hone J, Llaguno M C, Nemes N M, Johnson A T, Fischer J E, Walters D A, Casavant M J, Schmidt J and Smalley R E 2000 *Appl. Phys. Lett.* **77** 666
- [16] Aliev A E, Lima M H, Silverman E M and Baughman R H 2010 *Nanotechnology* **21** 035709

- [17] Hu L J, Liu J, Liu Z, Qiu C Y, Zhou H Q and Sun L F 2011 *Chin. Phys. B* **20** 096101
- [18] Berber S, Kwon Y K and Tomanek D 2000 *Phys. Rev. Lett.* **84** 4613
- [19] Maruyama S 2002 *Physica B* **323** 193
- [20] Alaghamandi M, Algaer E, Bohm M C and Muller-Plathe F 2009 *Nanotechnology* **20** 115704
- [21] Hou Q W, Cao B Y and Guo Z Y 2009 *Acta Phys. Sin.* **58** 7809 (in Chinese)
- [22] Zhang W, Zhu Z Y, Wang F, Wang T, Sun L and Wang Z 2004 *Nanotechnology* **15** 936
- [23] Hu G J and Cao B Y 2012 *Mol. Simul.* **38** 823
- [24] Feng D L, Feng Y H, Chen Y, Li W and Zhang X X 2013 *Chin. Phys. B* **22** 016501
- [25] Evans D J 1982 *Phys. Lett. A* **91** 457
- [26] Hoover W G 1983 *Annu. Rev. Phys. Chem.* **34** 103
- [27] Muller-Plathe F 1997 *J. Chem. Phys.* **106** 6082
- [28] Hulse R J, Rowley R L and Wilding W V 2005 *Int. J. Thermophys.* **26** 1
- [29] Terao T and Muller-Plathe F 2005 *J. Chem. Phys.* **122** 081103
- [30] Cao B Y 2008 *J. Chem. Phys.* **129** 074106
- [31] Cao B Y and Li Y W 2010 *J. Chem. Phys.* **133** 024106
- [32] Nose S 1984 *Mol. Phys.* **52** 255
- [33] Hoover W G 1985 *Phys. Rev. A* **31** 1695
- [34] Brenner D W 1990 *Phys. Rev. B* **42** 9458
- [35] Saito R, Matsuo R, Kimura T, Dresselhaus G and Dresselhaus M S 2001 *Chem. Phys. Lett.* **348** 187
- [36] Kapitza P L 1941 *J. Phys. (USSR)* **4** 181
- [37] Zhong H and Lukes J R 2006 *Phys. Rev. B* **74** 125403
- [38] Evans W J, Shen M and Keblinski P 2012 *Appl. Phys. Lett.* **100** 261908
- [39] Hu G J and Cao B Y 2013 *J. Appl. Phys.* **114** 224308